16 May 2001

Micromagnetic simulations of magnetization reversal in Co/Ni multilayers

V. D. Tsiantos[a], T. Schrefl[a], D. Suess[a], W. Scholz[a], J. Fidler[a], and J. M. Gonzales[b]

[a] Vienna University of Technology, Institute of Applied and Technical Physics, Wiedner Hauptstrasse 8-10/137, A-1040, Vienna, Austria.

[b] Instituto de Ciencia de Materiales de Madrid CSIC, Cantoblanco, 28049 Madrid, Spain.

In this paper the magnetization reversal process of Co/Ni/Co trilayers was studied using finite element micromagnetic simulations. Demagnetization curves were calculated for a multilayer with a Co layer thickness of 5 nm and a Ni layer thickness of 15 nm. Both the Ni and the Co layer reverse at the same well-defined switching field. A two-step process occurs at interlayer exchange lower than one third of the bulk value. The transition from a one-step to a two-step reversal process occurs if the anisotropy of Co is considerably high (Ku = 450 kJ/m³). A completely different reversal mechanism occurs if the uniaxial anisotropy of the Co layer approaches 45 kJ/m³. Now demagnetizing effects override the uniaxial anisotropy.

Keywords: micromagnetics, multilayers, finite elements.

Corresponding author: V. D. Tsiantos, Vienna University of Technology, Institute of Applied and Technical Physics, Wiedner Hauptstrasse 8-10/137, A-1040, Vienna, Austria. FAX: 0043-1-58801-13798. Email: v.tsiantos@computer.org

1. Introduction

Magnetic sensors and magneto-electronic devices are based on magnetic nanostructures. Their application requires a well-defined switching behaviour which can be tailored changing either the microstructure or the intrinsic magnetic properties. The magnetization reversal process of Co/Ni/Co trilayers was studied using finite element micromagnetic simulations. Work on CoNi multilayers has been done previously by a number of authors [1-4].

A uniaxial anisotropy parallel to the film plane was assumed within the Co layer, whereas zero anisotropy was used to mimic the properties of Ni. This system is a perfect model to investigate the role of anisotropy and interphase exchange on the magnetization reversal process in exchange spring magnets [5-8]. Indeed, the typical behaviour of a nanostructured, exchange coupled system is observed. Demagnetization curves were calculated for a multilayer with a Co layer thickness of 5 nm and a Ni layer thickness of 15 nm. Thus the net magnetization of a Co and a Ni layer are the same, since the spontaneous magnetization of Co is about three times larger than that of Ni. The computational region was a 200 nm x 200 nm with free boundary condition (Figure 1). The calculations were performed for two sets of samples with different Co anisotropy constant. The range of the intrinsic magnetic properties studied is given in Table 1. In addition to the quasi-static behaviour, the numerical integration of the Landau-Lifshitz-Gilbert equation shows how the reversed domains are formed as a function of time.

2. Model and Simulation Method

In micromagnetics the magnetic polarization is assumed to be a continuous function of space. The time evolution of the magnetization follows the Gilbert equation of motion.

$$\frac{d\mathbf{J}}{dt} = -|\gamma_0|\mathbf{J}\times\mathbf{H}_{eff} + \frac{\alpha}{J_s}\mathbf{J}\times\frac{\partial\mathbf{J}}{\partial t} \tag{1}$$

which describes the physical path of the magnetic polarization $\boldsymbol{J}$ towards equilibrium. The effective field $\boldsymbol{H}_{\text{eff}}$ is the negative functional derivative of the total magnetic Gibb's free energy, which can be expressed as the sum of the exchange energy, the magneto-crystalline anisotropy energy, the magnetostatic energy, and the Zeeman energy [9]. The term γ_0 is the gyromagnetic ratio of the free electron spin and α is the damping constant. To solve the Gilbert equation numerically the magnetic particle is divided in finite elements. A hybrid finite element boundary element method [10], is used to calculate the scalar potential u on every node point of the finite element mesh. The demagnetizing field, which contributes to the effective field, is the negative derivative of the scalar potential u. The effective field H^{i}_{eff} at the node point i of an irregular finite element mesh can be approximated using the box scheme

$$\mathbf{H}_{\text{eff,i}} = -\left(\frac{\delta E_t}{\delta\mathbf{J}}\right)_i = -\frac{1}{V_i}\frac{\partial E_t}{\partial\mathbf{J}_i}, \text{ for } V_i\to 0, \tag{2}$$

where V_{i} is the volume of the surrounding node i, such that

$$\sum_i V_i = V, \text{ and } V_i \cap V_j = 0 \text{ for } i\neq j, \tag{3}$$

The discretization of the Gilbert equation leads to an ordinary differential equation for every node for each component. In the case of a non-stiff problem it is advisable to use an appropriate method, such as Adams [11], whereas in stiff problems a backward differe-ntiation formulae (BDF) method could be an option for the time integration. BDF method

is implicit, so at each time step a non-linear algebraic system must be solved. For the solution of the non-linear system a method, such as Newton, has to be used which leads usually to a very large system of linear equations. In this paper the latter is solved using the scaled preconditioned incomplete generalised minimum residual method (SPIGMR) [12], based on GMRES (generalized minimum residual method) proposed by Youcef Saad [13]. SPIGMR belongs to the family of Krylov subspace methods, which are iterative methods for solving systems of linear equations. SPIGMR has been explored in micromagnetics by Vassilios D. Tsiantos *et al* [14,15].

A non-stiff method (Adams) and a stiff one (backward differentiation formulae, BDF) have been used to measure the stiffness of the problem. For the latter the ratio of the total number of time steps (nst) taken by the two solvers, that is nst(Adams)/nst(BDF), has been used. Note that the simulation time has to be the same in order to have a fair comparison [16]. The abovementioned method has been proposed to approximate numerically the stiffness of a system of ordinary differential equations (ODEs) in micromagnetics by Vassilios Tsiantos and James Miles [17]. For the stiffness we considered the case that $A^{*}=1.0\text{x}10^{-11}$ J/m, the crystalline anisotropy of Co is $K_1=4.5\text{x}10^{5}$ J/m^3, J_s(Co)=1.76T, and J_s(Ni)=0.628T. We found that the ratio of the time steps is 8406/879=9.56, that is BDF is around ten times faster. The simulation time considered was 5.1 ns for both simulations. The large ratio means that Co/Ni/Co simulations are stiff. However, another factor that has to be considered is the cost of each method per time step. The cost of the Adams method is given by the ratio of the total number of function (field) evaluations (nfe) per total number of time steps, which is 15292/8406=1.82. The cost of the BDF method for the unpreconditioned BDF method is approximately equal to the same ratio, that is the total nfe per total nst, which is 6625/879=7.54. It can be seen

that BDF has higher cost and this compensates the high number of time steps, however, the CPU time for the Adams is 6878.3 and for the BDF is 2338.6, that is a ratio of 2.94, which means that the case is stiff and a BDF method should be used.

3. Results

The simulations were performed for different values of the Co anisotropy constants. In a first set of simulations the uniaxial anisotropy constant of Co was assumed to be $K_1 = 450$ kJ/m^3 which corresponds to the bulk value. However, magnetic measurements [4] suggest much smaller effective anisotropy constant in the multilayer structure.

3.1 *High anisotropy film*

In addition to the interplay between anisotropy and exchange, the demagnetization field from the edges significantly influences the reversal process. Figure 2 shows two distinct reversal processes depending on the strength of the interlayer exchange. To model the influence of interlayer exchange the exchange constant of Ni was reduced from $A^* = 10^{-11}$ J/m to $A^* = 10^{-12}$ J/m in a 5 nm thick region next to the Co layer. Exchange hardening of the Ni layer provides a one-step reversal process if $A^* > 0.2 \times 10^{-11}$ J/m. Both the Ni and the Co layer reverse at the same well-defined switching field. A two-step process occurs at interlayer exchange lower than one third of the bulk value. The Ni layer reverses its magnetization at a low opposite field and the magnetization of the Co keeps its initial direction. The already reversed Ni layer stabilizes the magnetization of the Co layer owing to magnetostatic interaction which leads to an increase of the coercive field as compared to the high exchange coupled systems. Figure 3 gives the magnetization pattern in the middle of the sample at the beginning of the simulation and Figure 4 at $H_{ext} = -200$ kA/m for weak interlayer exchange. A further reduction of the interlayer exchange causes

vortex like structure during reversal (Fig. 5). The external field causes a nonuniform magnetic state within the Ni layer whereas the magnetization within the Co layer remains nearly parallel to the anisotropy axis. The transition from a one-step to a two-step reversal process occurs if the anisotropy of Co is considerably high (Ku = 450 kJ/m³).

3.2 *Low anisotropy film*

A completely different reversal mechanism occurs if the uniaxial anisotropy of the Co layer approaches 45 kJ/m³. Now demagnetizing effects override the uniaxial anisotropy. The Co layer reversed at lower opposing field, owing to its high magnetization. The remanence and the coercive field of the multilayer systems decrease with increasing interlayer exchange constant between the layers. In order to reduce the magnetostatic energy end domains are formed at zero applied field. The end domains become more pronounced with increased interlayer exchange which in turn facilitates magnetization reversal (Figure 6). In addition to the quasi-static behaviour, the numerical integration of the Landau-Lifshitz-Gilbert equation shows how the reversed domains are formed as a function of time. Figure 7 presents the demagnetizing curves for different values of Co anisotropy.

Acknowledgement

This work was supported by the Austrian Science Fund (projects Y132-PHY), and the Austrian Academic Exchange Program (project 4/2000).

References

[1] A. Salcedo *et al*, J. Magn. Magn. Mater. 196-197 (1999) 99.

[2] O.A Chubykalo, and J.M. Gonzalez, J. Magn. Magn. Mater. 196-197 (1999) 810.

[3] A. Hernando *et al*, J. Magn. Magn. Mater. 221 (2000) 172.

[4] F.J. Palomares *et al*, J. Magn. Magn. Mater. (in press).

[5] K. Mibu *et al*, J. Magn. Magn. Mater. 163 (1996) 75.

[6] K. Mibu *et al*, Phys. Rev. B 58 (1998) 6442.

[7] E. E. Fullerton *et al*, Phys. Rev. B 58 (1998) 12193.

[8] E. E. Fullerton *et al*, Appl. Phys. Lett. 72 (1998) 380.

[9] W. F. Brown, Jr., *Micromagnetics* (Wiley, New York, 1963).

[10] D. R. Fredkin and T. R. Koehler, IEEE Trans. Magn. 26 (1990) 415.

[11] C. William Gear, *Numerical Initial Value Problems in Ordinary Differential Equations* (Prentice-Hall, Englewood Cliffs, 1971).

[12] P. N. Brown and A. C. Hindmarsh, J. Appl. Math. Comp. 31 (1989) 40.

[13] Y. Saad and M. H. Schultz, SIAM J. Sci. Stat. Comp. 7 (1986) 856.

[14] V. D. Tsiantos *et al*, in: Proceedings of the 3rd European Conference Numerical Mathematics and Advanced Applications, ed. P. Neittaanmaki *et al* (World Scientific, Singapore, 2000) pp. 743-752.

[15] V. D. Tsiantos *et al*, Int. J. Nonlin. Scie. Num. Sim, 2001 (submitted).

[16] V. D. Tsiantos *et al*, J. Appl. Phys. 89 (2001) 7600.

[17] V. D. Tsiantos, and J.J. Miles, in: Proceedings of the 16th IMACS World Congress 2000 on Scientific Computation, Applied Mathematics and Simulation, August 21-25, 2000, Lausanne, Switzerland.

Table 1. Intrinsic parameters used for the simulations.

		Js (T)	A (J/m)	A^* (J/m)	K_1 (kJ/m^3)
High anisotropy film	*Co*	1.76	1.3×10^{-11}		450×10^3
	Ni	0.628		1.0×10^{-11} to 0.1×10^{-11}	0.0
Low anisotropy film	*Co*	1.76	1.3×10^{-11}		4.5×10^3 to 45×10^3
	Ni	0.628		0.5×10^{-11}	0.0

List of figure captions

Figure 1. Geometry of Co/Ni/Co sample.

Figure 2. Demagnetising curves varying the interlayer exchange constant A^* for the Ni layers next to the Co, given in J/m, and Js(Ni)=0.628 T.

Figure 3. Magnetisation distribution ($A^*=10^{-11}$ J/m, $H_{ext}=0$).

Figure 4. Magnetisation distribution ($A^*=10^{-11}$ J/m, H_{ext}=-200 kA/m).

Figure 5. Magnetisation distribution ($A^*=0.2x10^{-11}$ J/m, H_{ext}= -173 kA/m, K_1=450 kJ/m^3).

Figure 6. Demagnetising curves for various values of Co anisotropy ($A^*=0.5x10^{-11}$ J/m).

Figure 7. Magnetisation distribution for low Co anisotropy ($K_1=4.5x10^3$ J/m^3, H_{ext}=-11 kA/m, $A^*= 0.5x10^{-11}$ J/m).

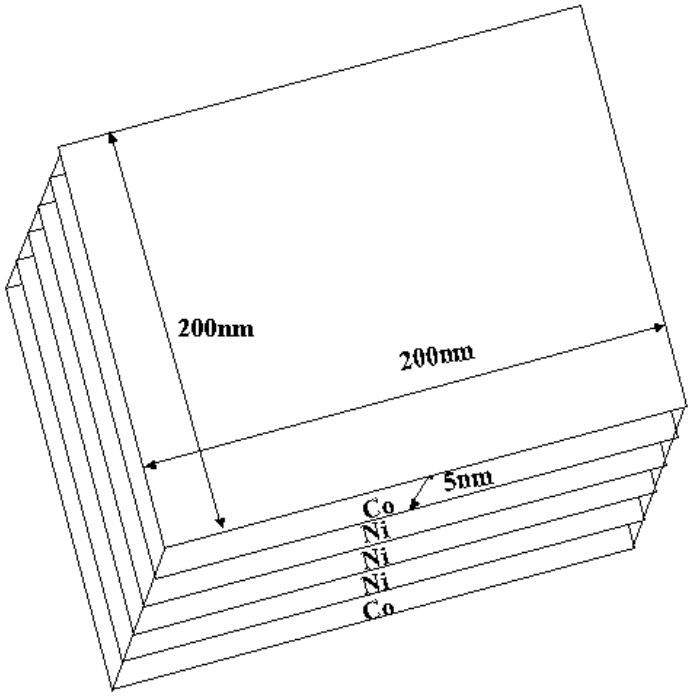
200nm
200nm
5nm
Co
Ni
Ni
Ni
Co

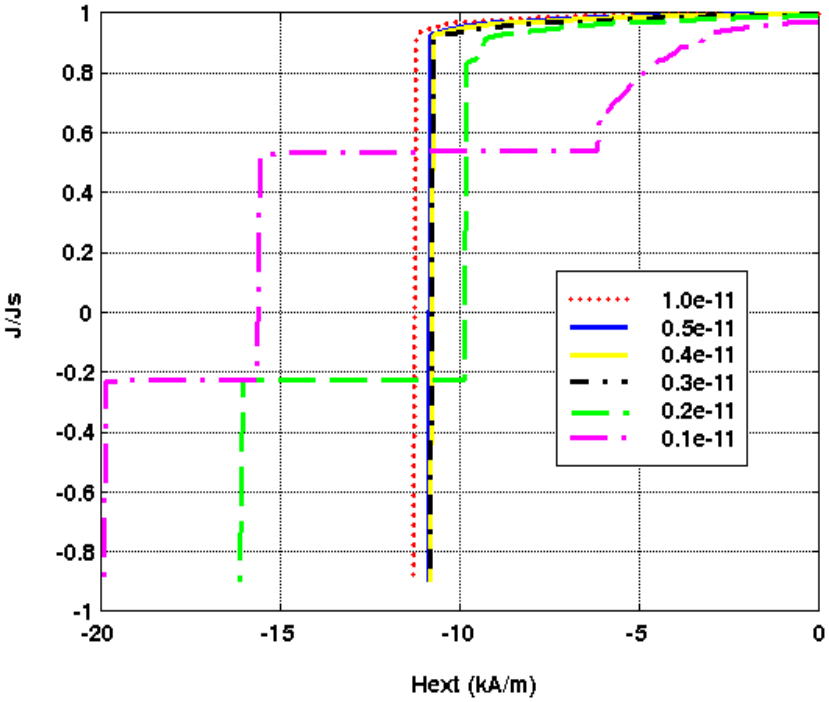
1
0.8
0.6
0.4
0.2
0
-0.2
-0.4
-0.6
-0.8
-1
-20
-15
-10
-5
0
J/Js
Hext (kA/m)
1.0e-11
0.5e-11
0.4e-11
0.3e-11
0.2e-11
0.1e-11

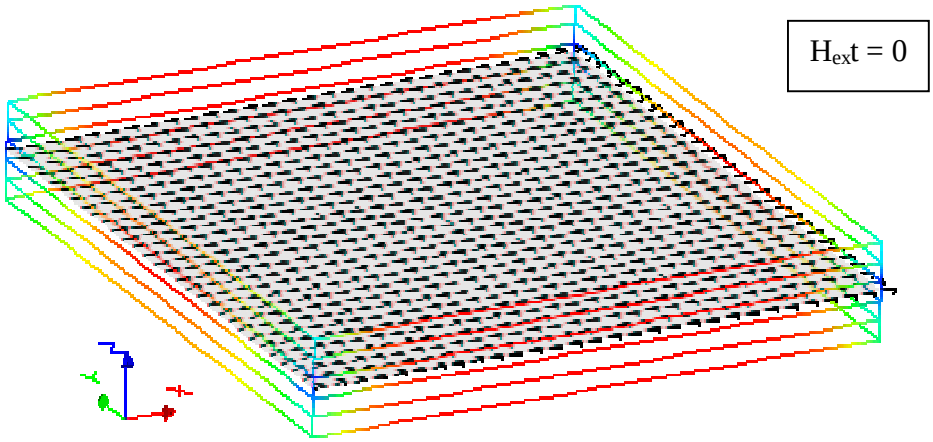
$H_{ext} = 0$

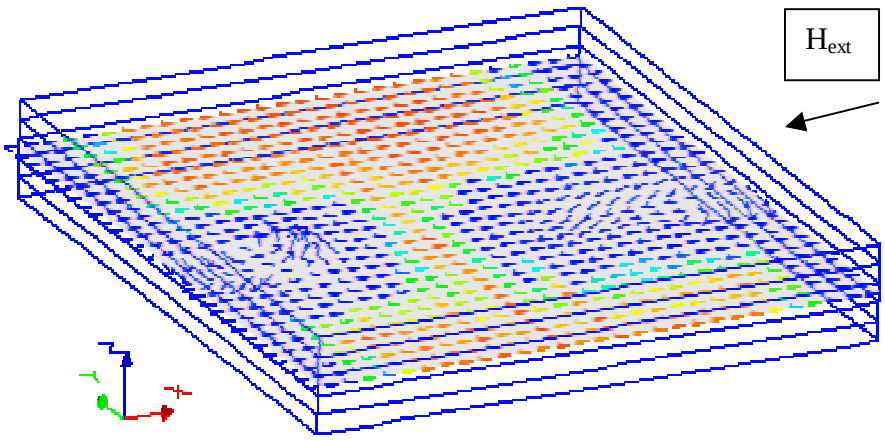
H_{ext}

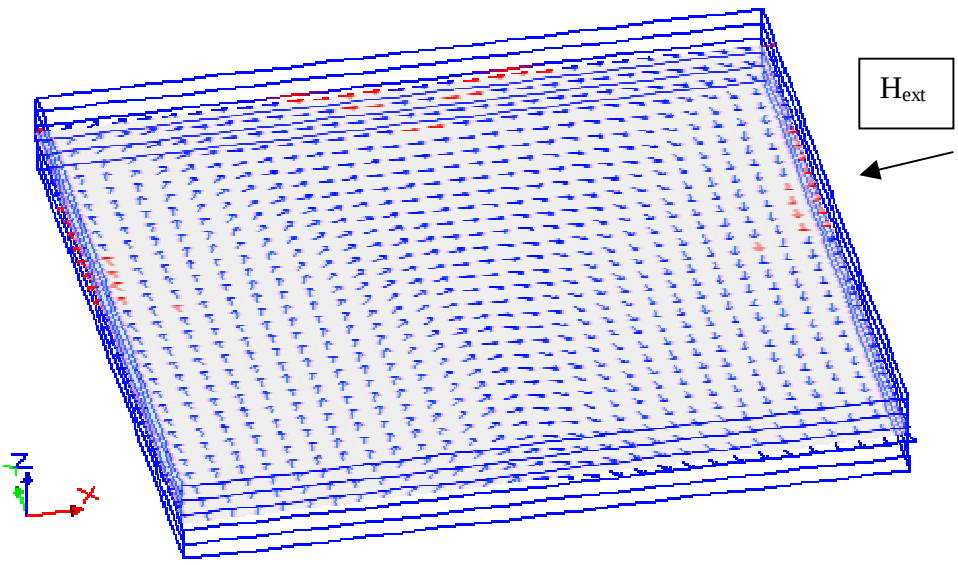
H_{ext}
Z
X

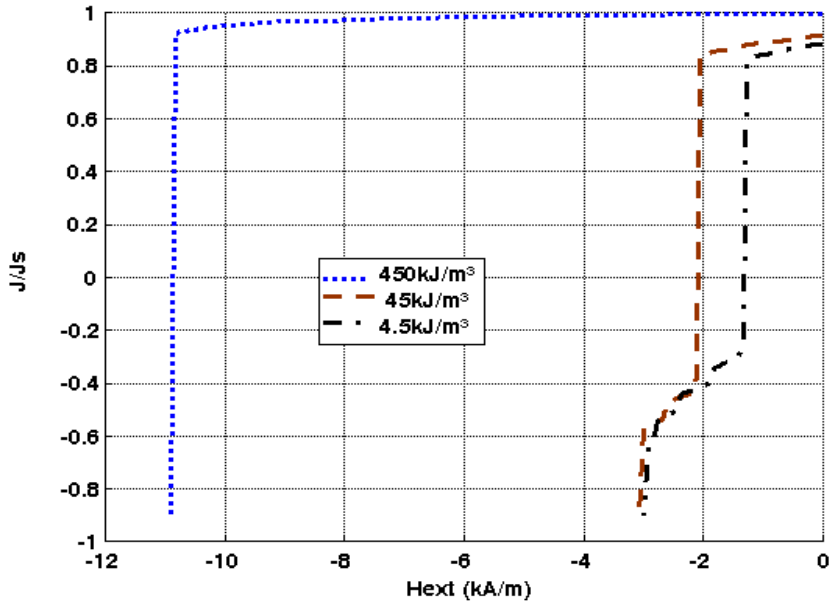
1
0.8
0.6
0.4
0.2
0
-0.2
-0.4
-0.6
-0.8
-1
J/Js
-12
-10
-8
-6
-4
-2
0
Hext (kA/m)
450kJ/m3
45kJ/m3
4.5kJ/m3

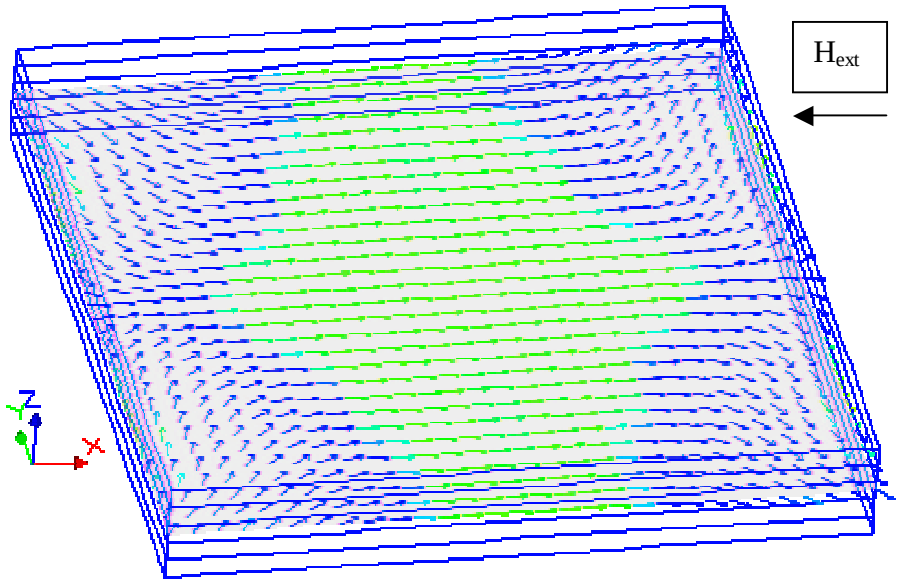
H_{ext}
Y
X